THE JOURNAL OF PHYSICAL CHEMISTRY C

ARTICLE

pubs.acs.org/JPCC

Cosolvent-Induced Gelation and the Hydrothermal Enhancement of the Crystallinity of Titania−Silica Mixed Oxides for the Photocatalytic Remediation of Organic Pollutants

Harrison S. Kibombo,* Dan Zhao, Andra Gonshorowski, Sridhar Budhi, Miles D. Koppang, and Ranjit T. Koodali*

Department of Chemistry, University of South Dakota, Vermillion, South Dakota 57069, United States

ABSTRACT: The photocatalytic activity of hydrothermally synthesized TiO_2−SiO_2 mixed oxides was examined in this study. Powder X-ray diffractometry, nitrogen adsorption, diffuse reflectance spectrometry, Raman, and UV−vis spectrometry demonstrated that the pore geometries and the nature of the crystal phase can be tailored by cosolvent-induced gelation (CIG) in the synthesis of mixed oxide materials. This body of work attempts to support the role of crystallinity enhanced by the hydrothermal synthesis (HTS) in establishing active sites pertinent to the advanced oxidation process (AOP) in TiO_2−SiO_2 mixed oxide materials.

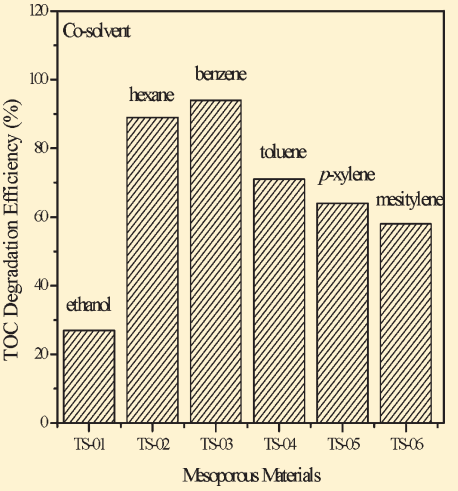

1. INTRODUCTION

Accidents, spills, leaks, improper disposal, and handling of hazardous wastes have resulted in thousands of sites across our country with contaminated land, water, and air. A recent assessment by the Environment Protection Agency (EPA) and its partners in 2008 illustrated the dire need for cleanup programs and initiatives to curb and destroy organic waste pollutants before their discharge into the environment. Increased public concern has prompted the development of novel treatment methods, with photocatalysis emerging as a fast-growing research area in the field of pollutant degradation. Current treatment methods such as adsorption by activated carbon and air stripping have proved inefficient because they do not convert the pollutants into innocuous wastes.[1] The photocatalytic process is believed to be superior to these existing technologies due to high degradation efficiencies and complete breakdown of toxic organic wastes to environmentally benign products.

Waste water derived from different chemical industries such as petrochemical, resin manufacturing, and paper making usually has high concentrations of phenol and its derivatives. It has been determined that prolonged skin exposure to phenol may lead to severe burns, and the ingestion or inhalation of its vapors is associated with carcinogenic effects on the lungs and central nervous system.[2] Recent research efforts illustrate the degradation of phenolic compounds by the heterogeneous advanced oxidation process (AOP) using suspensions of semiconductor nanoparticles.[3,4] Among these, titania (TiO_2) is the most widely used photocatalyst due to its low cost, high stability, and high activity. The relatively low surface areas and porosities of pure titania have prompted research toward finding methods to alleviate these barriers. Several authors have opted to utilize silica (SiO_2) as an adsorbent or support due to its uncharged framework and moderate hydrophobicity allowing preconcentration of the organic material near the photoactive sites.[5] Elaborate procedures such as coprecipitation, flame hydrolysis, impregnation, and chemical vapor deposition have indicated that the interaction of TiO_2 with SiO_2 generates a material with new catalytically active sites, possessing enhanced thermal and mechanical stability due to the presence of the supporting SiO_2 phase.[6,7] Sol−gel technology has proved to be more practical and economical than its competitors because it provides versatility in tuning the physiochemical properties of the inorganic oxides during the preparation process.[8−10] In an effort to ascertain fine control of the formation of the structure, the use of hybrid polymers,[11] alkoxide bridging ligand complexes,[12,13] and structure-directing agents has also been incorporated with sol−gel

Received: November 17, 2010
Revised: February 17, 2011
Published: March 07, 2011

synthesis. However, these methods often introduce residual ion impurities into the mesostructure.[14,15] Owing to the existing complexities in interpreting the photocatalytic degradation mechanisms of organic molecules,[16] there is still a search for more efficient porous materials with high purity and superior catalytic efficiencies for the oxidation of various organic pollutants. The performance of these inorganic oxides is largely attributed to preparation methods and synthesis conditions through which homogeneity, crystallinity, crystal size, and surface area can be optimized.[17−20] A more economically viable approach has been to utilize different combinations of solvent systems in the manipulation of the mesostructure. Warrier and co-workers have illustrated that the sol−gel chemistry in an alcohol solvent system greatly influences the hydrolysis of metal alkoxide precursors, thus improving the textural properties of the mixed oxide materials.[21] With the comparison of a series of alcohols, Xu et al. showed that the photoactivity of supported TiO_2 on SiO_2 for the degradation of acetophenone was superior when its synthesis was conducted in an ethanol medium.[22] However, mixed oxides synthesized in a single-solvent media appear to be limited to inferior textural properties and low catalytic activity. This work relays an exploration of a combination of techniques that simultaneously improves the texture and surface properties of the mixed oxide catalyst within a one-pot synthesis. Of the approaches investigated, none, to the best our knowledge, has ventured into hydrothermally synthesized, cosolvent-induced mixed TiO_2−SiO_2.

The difference in hydrolysis and condensation rates of the SiO_2 and TiO_2 alkoxide precursors results in the accumulation of separate titanium-rich microdomains and inhomogeneous TiO_2−SiO_2 mixed oxides. More homogeneity can be achieved by prehydrolyzing the Si alkoxide with water and nitric acid in an organic solvent system prior to the addition of the Ti alkoxide and, as a result, produce catalytically active Ti−O−Si heterolinkages. Our approach is to accelerate the gelation rate dramatically from several days[23] to a few minutes by the introduction of an aromatic cosolvent so that the two hydrolyzing metal alkoxides gel together. An added advantage of the nonpolar cosolvent is that it minimizes the surface tension of the pore walls, leading to the formation of a more open porous structure and high-surface-area materials in a limited amount of time.[24] Materials bearing these mixed phases present at the interface region have shown enhanced catalytic activity for the oxidation of phenol.[5]

Our photocatalytic studies indicate a superior catalytic activity of TiO_2−SiO_2 compared to that of commercially available TiO_2, and these efficiencies could be attributed to the increased surface area, high crystallinity, and dispersion of TiO_2. Preliminary studies in our laboratory pertaining to TiO_2−SiO_2 mixed oxides synthesized at room temperature (without hydrothermal treatment) have exhibited low photocatalytic efficiency mainly due to low crystallinity. Bein and colleagues[25] utilized electron microscopy in conjunction with in situ dynamic light scattering (DLS) and X-ray diffraction (XRD) to understand the importance of the crystalline structure within amorphous gel particles during the hydrothermal treatment as a means of illustrating the significance of crystallinity in harnessing the catalytically active features of porous gel materials. This treatment is vital in accelerating the morphological transformation from a random gel structure to islands of regular crystal lattice from several weeks to as little as half of a day.

We employ the hydrothermal synthesis (HTS) as it is efficient in achieving highly stable crystalline materials at relatively low temperatures in a closed system.[26−28] It is believed that anatase phases with small particle sizes and high crystallinity produce the most active photocatalysts in the degradation of organic substrates.[29] Because phase transformation from anatase to rutile at elevated calcination temperatures is accompanied by the agglomeration of TiO_2 crystallites that retard photocatalytic activity, the integration of the SiO_2 phase is essential in ensuring that the presence of dispersed anatase crystallites is maintained.

During the photocatalysis process, illumination of the titania−silica (TiO_2−SiO_2) semiconductor catalyst with ultraviolet (UV) radiation activates the catalyst, creating a redox environment necessary for mineralization. The combination of increased surface area, high crystallinity, and dispersion increases the number of active sites that interact with surface-adsorbed molecules and hydroxyl groups available for participation in the photoredox reaction.

2. EXPERIMENTAL METHODS

2.1. Materials. Commercially available titanium isopropoxide $Ti(OCH(CH_3)_2)_4$ (Acros, 98+%), tetraethylorthosilicate $Si(OC_2H_5)_4$ (Acros, 98%), ethanol (Pharmco-AAPER, A.C.S/USP grade, anhydrous), toluene (ACS grade), phosphoric acid (Sigma-Aldrich >85% wt solution in water, ACS grade), conc. nitric acid (Acros, ACS grade), hydroquinone (Sigma, >99%), benzoquinone (TCI America, 98%), 1,2,4-benzenetriol (Acros), methanol (Acros, 99.9% HPLC grade), phenol (Acros, 99+%, ACS grade), and Aeroxide TiO_2 P 25 (Evonik Degussa) were used as received. Deionized water (resistivity > 18 MΩ·cm) was used throughout the experiments.

2.2. Synthesis of Wet Gels. A series of TiO_2−SiO_2 mixed oxide sols were prepared by simultaneous hydrolysis and condensation of metal alkoxides $Si(OC_2H_5)_4$ and $Ti(OCH(CH_3)_2)_4$. A hydrothermal treatment was performed to complete the synthesis procedure and induce crystallization. In a typical synthesis, 1.65 mL of $Si(OC_2H_5)_4$ was added slowly into a solution containing 9 mL of toluene dissolved in 9 mL of C_2H_5OH (200 proof, anhydrous) under vigorous stirring in a Teflon linear. The hydrolysis process was initiated by the introduction of 1 mL of H_2O and catalyzed by the addition of 100 μL of conc. HNO_3. $Ti(OCH(CH_3)_2)_4$ was added dropwise to ensure homogeneous distribution and the suspension left to stir until gelation. Gelation was usually achieved in less than 3 h. The resultant gels were subjected to hydrothermal treatment in a Thermolyne autoclave reactor furnace and heated to a temperature of 120 °C for 14 h, filtered, and dried overnight at 70 °C. These powders were then ground and calcined in static air at 500 °C for 6 h at a heating rate of 3 °C/min.

2.3. Characterization. The calcined samples were characterized by X-ray powder diffraction with a Scintag Pad V X-ray diffractometer with DSMNT data acquisition and analysis software or a Rigaku Ultima IV with PDXL software. The diffraction patterns were recorded at room temperature using a Ni filtered Cu Kα radiation (λ = 1.5408 Å), and an accelerating voltage of 40 kV and emission current of 44 mA were employed. The angle regions were scanned from 20 to 75° (2θ) with a step size of 0.02°. The textural properties such as surface area and pore size distribution of the mixed oxide materials were measured using N_2 physisorption measurements. After the samples were dried overnight at 70 °C and degassed at 100° for at least 1 h, N_2 adsorption−desorption isotherms were obtained at 77 K using

a NOVA 2200*e* (Quantachrome Instruments) surface area and pore size analyzer. The surface areas were calculated by using the Brunauer−Emmett−Teller equation within a relative pressure range (P/P_0) of 0.05−0.30. The pore volume was determined from the amount of nitrogen adsorbed at the highest relative pressure of $P/P_0 \approx 0.99$. The pore diameter and pore size distribution plots were determined by applying the Barrett−Joyner−Halenda (BJH) model to the desorption isotherm. The Raman spectra were acquired with a Horiba Jobin Yvon LabRam ARAMIS spectrophotometer with an internal HeNe (633 nm) excitation laser. The unfiltered beam of scattered laser radiation was focused onto the sample through a microscope objective (×50) for an acquisition time of 10 s and repetition of 10×. The radiation was then dispersed by an 1800 line/mm grating onto a CCD detector. The diffuse reflectance (DR) spectra of the samples were recorded in the range of 190−700 nm using a Cary 100 Bio UV−Vis spectrophotometer equipped with a Harrick DR praying mantis accessory. Fourier transform infrared (FT-IR) spectroscopy studies were constituted by drying the samples and potassium bromide (KBr) in the oven overnight at 80−90 °C to eliminate moisture. KBr was ground into a fine powder using a mortar and pestle and compacted into a pellet by applying hydraulic pressure. This pellet was then used to record the background spectra. For analysis, about 100 mg of KBr and 2−3 mg of the sample of interest were ground together, and the pellet obtained was used for obtaining FT-IR spectra. A MIDAC FT-IR instrument model M2000 using MIDAC-EZ software was used to record the infrared spectra of the TiO_2−SiO_2 mixed oxides.

2.4. Photocatalysis of TiO_2−SiO_2. The photocatalytic activity of the prepared mixed oxide catalysts was assessed by monitoring the degradation of phenol from aqueous suspensions. Catalyst (30 mg) was dissolved in 30 mL of phenol solution (2×10^{-4} M) in a quartz cylindrical jacket reactor at an initial pH of 4−5. The suspensions were stirred at a rate of 300 rpm in the dark for 0.5 h to ensure adsorption−desorption equilibrium and purged with molecular oxygen at approximately 60 mL/min. The reaction temperature was kept constant at approximately 25 °C by channeling water between the double-walled reactor. Irradiation for 3 h was carried out by a xenon lamp (Newport 1000 W) through a Pyrex glass cut filter of 280 nm. These experimental conditions were maintained throughout the course of the experiment. After irradiation, the suspensions were centrifuged at 3200 rpm for 15 min and filtered through a 0.45 μm Millipore filter membrane, and the clear solutions were transferred to test tubes for analysis.

2.5. Photocatalytic Efficiency of TiO_2−SiO_2. An estimation of the amount of organics was determined using a Shimadzu TOC-V CSH total organic carbon analyzer immediately after filtration to confirm the catalytic activity of the mixed oxides.

3. RESULTS AND DISCUSSION

3.1. Effect of the Nature of Cosolvent. The high-angle X-ray diffractogram of calcined samples prepared using ethanol as a solvent (1:1 ratio) in combination with hexane, toluene, *p*-xylene, and mesitylene as nonpolar cosolvents is shown in Figure 1. The sample prepared using only ethanol (in the absence of any cosolvent) shows relatively broad peaks compared to the other four samples. Addition of cosolvents such as hexane, toluene, *p*-xylene, or mesitylene leads to small improvement in crystallinity. A noticeable difference can be observed in the

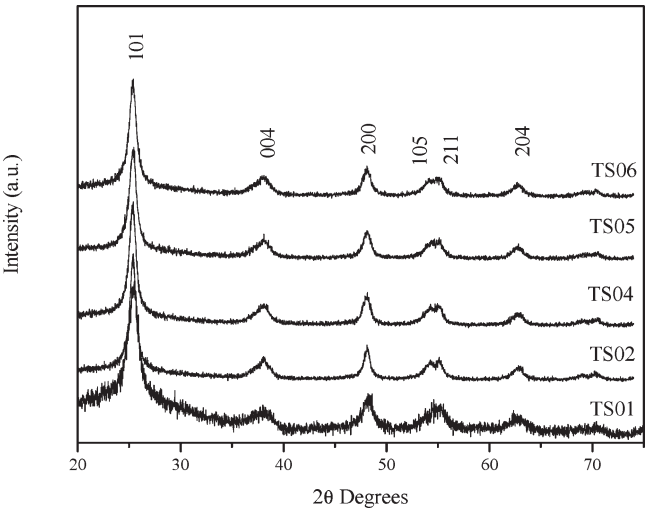

Figure 1. Wide-angle XRD patterns of select calcined TiO_2−SiO_2 materials. The ratio of ethanol/cosolvent is 1:1, in which the cosolvents for TS01, TS02, TS04, TS05, and TS06 are ethanol, hexane, toluene, *p*-xylene, and mesitylene, respectively.

disappearance of the broad shoulder between 27−35° (2θ) (due to amorphous SiO_2) in these four samples. In summary, all of the TiO_2−SiO_2 samples calcined at 500 °C show peaks that are due to the anatase phase of TiO_2. The sample prepared solely with ethanol (in the absence of a cosolvent) shows weak peaks because of the low diffraction contrast of the anatase spieces.[30]

The nitrogen isotherms of the TiO_2−SiO_2 mixed oxides prepared using ethanol/cosolvent ratios of 1:1 were examined, and the results are shown in Figure 2A. They exhibit type IV isotherms typical of mesoporous materials. A characteristic feature of mesoporous materials is the appearance of hysteresis, which is a reflection of the porosity of these materials and a consequence of pore filling and emptying taking place separately. Larger pores that may need to access their environment through smaller pores may experience capillary evaporation at pressures at which the smaller pore counterparts are still filled with gas molecules.[31] The initial part of the type IV isotherm is due to monolayer adsorption at low relative pressures. As the relative pressure increases, multilayer adsorption occurs and is followed by capillary condensation. After all of the pores are filled, the adsorption isotherm usually levels. The textural properties, including specific surface area, pore volume, and average pore diameter obtained from nitrogen adsorption−desorption analysis, are shown in Table 1.

The TiO_2−SiO_2 prepared by using only ethanol results in a hysteresis loop of H3 classification featuring parallel and almost horizontal adsorption and desorption branches, as shown in Figure 2A. H3 type loops are also often associated with morphologies of narrow slit-like pores of broad pore size distribution with irregular shaped particles. Cosolvent-induced gelation (CIG) results in TiO_2−SiO_2 displaying hysteresis loops of H3 type classification and do not level off at relative pressures close to the saturation vapor pressure. These H3 loop materials do not exhibit any limiting adsorption at high P/P_0, suggesting that the materials are comprised of aggregates (loose assemblages) of plate-like particles forming slit-like pores.[32] The desorption branch of these mixed oxide types contains a moderate region associated with gradual closure of the loop, suggesting a delayed

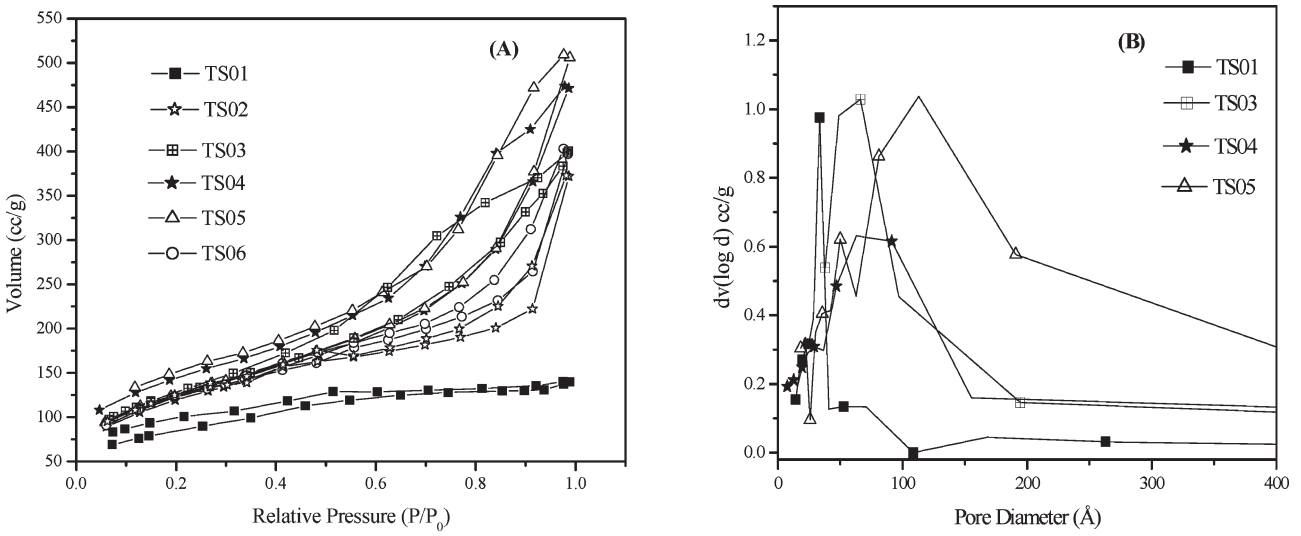

Figure 2. Nitrogen physisorption properties of representative calcined TiO_2-SiO_2 materials in which the ratio of ethanol/cosolvent is 1:1. Adsorption−desorption isotherms (A) and pore distributions (B) of materials whose cosolvents for TS01, TS02, TS03, TS04, TS05, and TS06 are ethanol, hexane, benzene, toluene, *p*-xylene, and mesitylene, respectively.

Table 1. Textural Properties of Cosolvent-Induced TiO_2-SiO_2 Mixed Oxide Materials

material	T/S[a] (mol/mol)	cosolvent	solvent/ cosolvent	S_{BET}[b] ($m^2\ g^{-1}$)	pore volume ($cm^3\ g^{-1}$)	ave. pore diameter (Å)	isotherm type	PSD[c]	band gap E_g^{eff} (eV)
TS01	1:1	ethanol	1:0	282.1	0.216	30.66	IV-H3	unimodal-n	3.05
TS02	1:1	hexane	1:1	425.9	0.577	54.16	IV-H3	trimodal-n	3.34
TS03	1:1	benzene	1:1	423.7	0.619	57.25	IV-H3	unimodal-n	3.19
TS04	1:1	toluene	1:1	423.3	0.729	68.89	IV-H3	trimodal-b	3.21
TS05	1:1	*p*-xylene	1:1	443.2	0.783	70.64	IV-H3	trimodal-b	3.26
TS06	1:1	mesitylene	1:1	430.9	0.614	57.04	IV-H3	trimodal-b	3.31
TS07	1:1	toluene	2:1	318.6	0.319	40.12	IV-H1	unimodal-n	3.21
TS08	1:1	toluene	1:2	273.6	0.439	64.18	IV-H3	unimodal-b	3.31
TS09	1:0	toluene	1:1	65.34	0.231	141.1	V-H3	unimodal-n	3.05
TS10	1:2	toluene	1:1	671.1	1.602	95.64	IV-H3	unimodal-b	3.34
TS11	1:3	toluene	1:1	671.5	1.611	95.94	IV-H3	unimodal-b	3.33
TS12	1:4	toluene	1:1	1033	1.771	68.56	IV-H3	unimodal-b	3.32
TS13	1:2	ethanol	1:0	507.1	0.372	29.31	IV-H3	unimodal-n	3.08
TS14	1:3	ethanol	1:0	529.8	0.379	28.60	IV-H3	unimodal-n	3.14
TS15	1:4	ethanol	1:0	634.4	0.458	28.87	IV-H3	unimodal-n	3.15

[a] The TiO_2-SiO_2 samples are referred to as TS with arbitrary numbers to assert chronological order. T/S refers to the molar ratio of TiO_2/SiO_2 in the gel. [b] Surface area determined by applying the Brunauer−Emmett−Teller (BET) equation to the adsorption isotherm. [c] Pore size distribution mode b and n refer to broad and narrow distribution, respectively.

evaporation of the liquid. Adsorption isotherms for certain porous solids may also exhibit unique pore size characteristics. Pore size distributions for selected samples are shown in Figure 2B. Others are not shown for the sake of clarity. TS01 prepared by only ethanol suggests a highly uniform set of pores with a BJH pore diameter of 37.91 Å and an average pore diameter of 30.66 Å, with a unimodal pore size distribution centered at 30 Å. The ability to adjust the pore sizes and tailor the surface properties is materialized in this study by the use of cosolvents. It can be observed that the addition of benzene results in photocatalysts, TS03, with a fairly unimodal distribution of pores of diameters centered around 60 Å, suggesting strong sorption interactions between the adsorbate and adsorbent surface.[31] Rapid gelation with toluene in TS04 leads to a hierarchically ordered set of pores with micro-, meso-, and macroparticles at 10, 30, and 80 Å, respectively. A trimodal distribution averaging at about 75 Å and a broad range of distributions greater than 150 Å is observed when *p*-xylene is introduced into the silica framework. The broader distribution of pores appears to be a recurring trend with addition of more substituted aromatic solvents. This factor is evident in the significantly larger pore volumes of cosolvent-induced samples as compared to those of the single-solvent samples. UV−vis DR was used to estimate the effective band gap of the TiO_2-SiO_2 materials, and the results are shown in Figure 3.

The absorption below 400 nm is mainly attributed to the electron transitions from the valence band to the conduction band. We observed a slight blue shift when cosolvent was induced

dx.doi.org/10.1021/jp110988j |*J. Phys. Chem. C* 2011, 115, 6126–6135

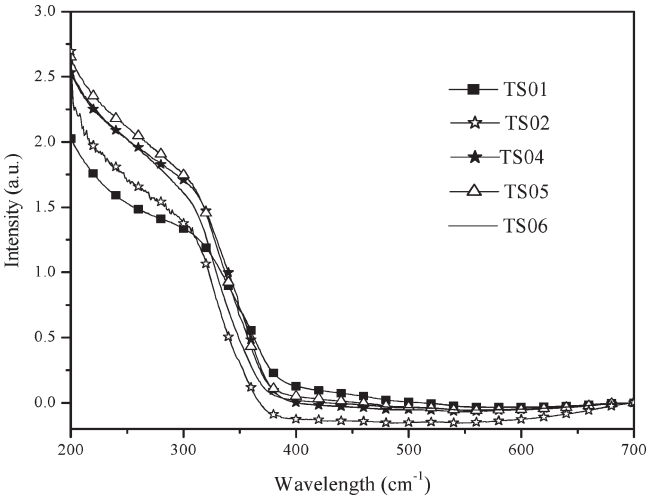

Figure 3. DR spectra for select calcined TiO_2-SiO_2 materials. The ratio of ethanol/cosolvent is 1:1, in which the cosolvents for TS01, TS02, TS04, TS05, and TS06 are ethanol, hexane, toluene, *p*-xylene, and mesitylene, respectively.

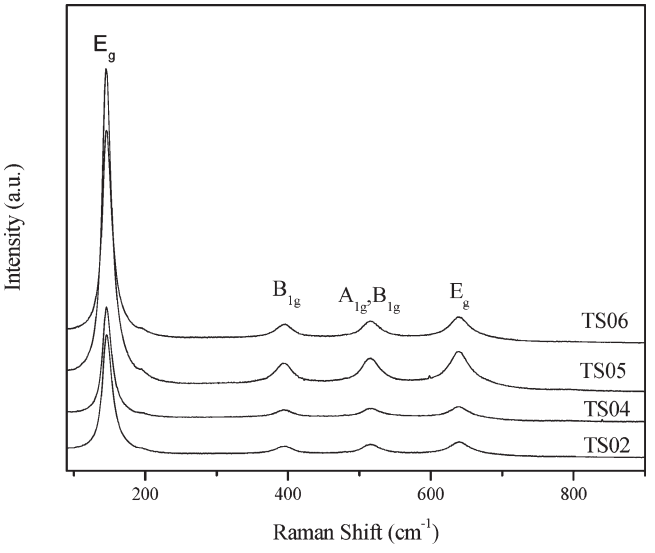

Figure 4. Raman Spectra for representative calcined TiO_2-SiO_2 materials. The ratio of ethanol/cosolvent is 1:1, in which the cosolvents for TS02, TS04, TS05, and TS06 are hexane, toluene, *p*-xylene, and mesitylene, respectively.

into the mesostrucuture, inferring a change in the crystallite size of the anatase TiO_2. The crystallite sizes of anatase could not be accurately calculated from powder XRD data using the Debye−Scherrer method. The presence of the silica phase creates considerable uncertainty in estimating the crystallite size of the titania phase alone. The band gap energy estimated from UV−vis DR spectra are also listed in Table 1. In order to investigate the crystalline nature of the TiO_2 phase, we utilized Raman spectroscopy due to its high sensitivity to detect small crystalline aggregates whose intensity of the bands is associated with the presence of anatase.

Although the factor group analysis predicts six Raman-active modes, Figure 4 illustrates samples calcined at 500 °C, each having four modes at 638, 510, 391, and 143 cm^{-1} with an additional shoulder at 197 cm^{-1}. Peaks at 638, 197, and 143 cm^{-1} may be due to E_g symmetric modes, and the peak at 510 cm^{-1} is due to two modes of B_{1g} and A_{1g} symmetry. More distinct peaks are observed with aromatic cosolvents as compared to their aliphatic counterparts. The Raman spectra indicate clearly that only the anatase phase of TiO_2 exist in these materials, which is consistent with powder XRD studies. These patterns suggest that the rutile phase was not formed, confirming the enhanced thermal stability of TiO_2 by the introduction of a restricting SiO_2 phase. Anderson and Bard[5] suggest that the ability of the surrounding SiO_2 lattice to lock the Ti−O species with the SiO_2 at the interface prevents the diffusion and nucleation that is necessary for the phase transformation of the anatase to the rutile form.

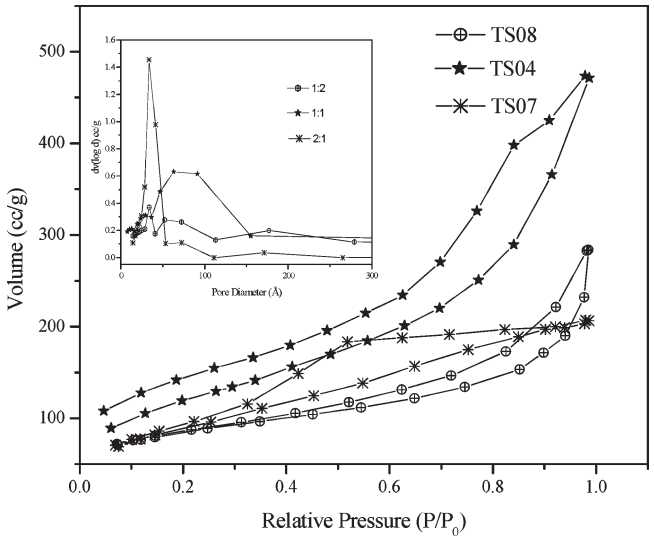

Figure 5. Nitrogen adsorption−desorption isotherms and pore size distributions (inset) of representative TiO_2-SiO_2 maintained at in the ratio of 1:1 but with the ratios of ethanol/toluene for TS04, TS07, and TS08 varied from 1:1, 2:1, and 1:2, respectively.

3.2. Effect of the Amount of Cosolvent on the TiO_2-SiO_2 Mesostructure. In this study, we observed that the nature of cosolvent can reflect on the uniformity and porosity of the resulting catalyst. Similar trends emerged where pore sizes were found to depend on the relative amounts of cosolvent in the gel synthesis. In order to accentuate and understand the above phenomenon, select catalysts were synthesized using varying amounts of toluene. This was the cosolvent of choice because of its ability to induce remarkably fast gelation (i.e., <30 min). Figure 5 illustrates the nitrogen adsorption−desorption isotherms of TiO_2-SiO_2 materials prepared with the same titania to silica ratios (1:1) but different solvent to cosolvent amounts. The TiO_2-SiO_2 material prepared with relatively low amounts of toluene, that is, a 2:1 ratio of ethanol/toluene, shows a type IV isotherm with H1 type hysteresis loop. The appearance of the H1 loop has been ascribed to porous materials with a fairly narrow and uniform pore size distribution. This is indicated in the inset plot in Figure 5. Increasing the amount of toluene to 1:1 leads to a type IV isotherm, which is true of mesoporous materials.[33] At higher relative pressures, the amount adsorbed does not level off, indicating the presence of macropores. In addition, the adsorption and desorption isotherms in this sample do not coincide at low relative pressures, indicating the presence of micropores.

dx.doi.org/10.1021/jp110988j |*J. Phys. Chem. C* 2011, 115, 6126–6135

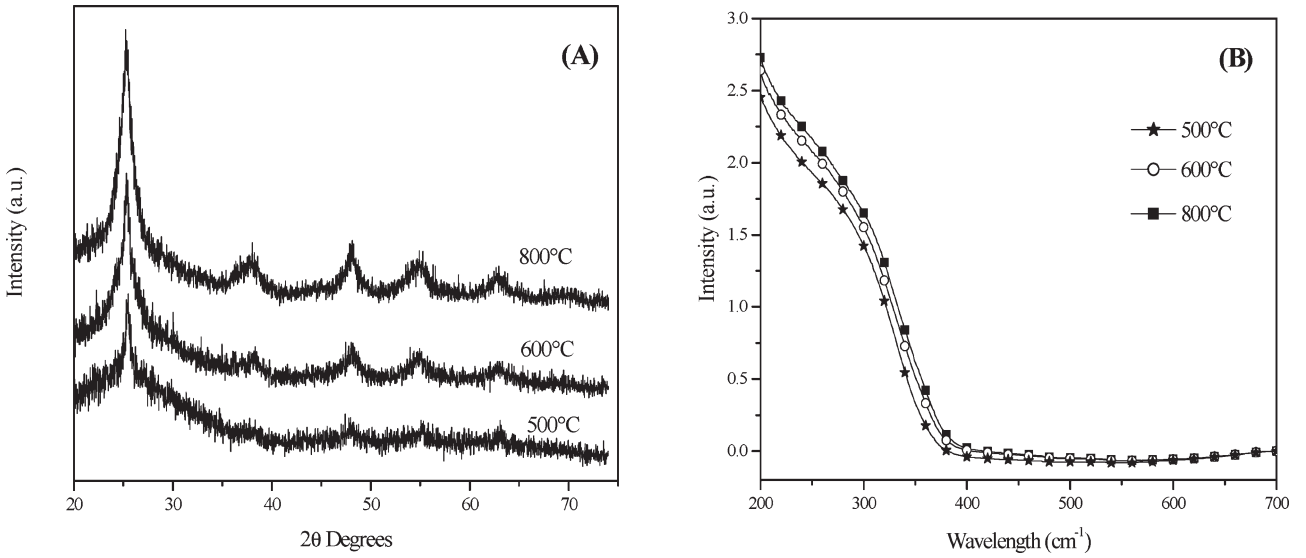

Figure 6. Wide-angle XRD (A) and DR spectra (B) of TiO_2-SiO_2 mixed oxide materials whose hydrolysis was catalyzed by aq. NH_3 and calcined at temperatures of 500, 600, and 800 °C.

The hysteresis loop is categorized as H3, which is reported for materials comprised of aggregates of particles shaped like plates forming slit-like pores. Increasing the toluene amount further to obtain a 1:2 ethanol/toluene ratio retains the H3 hysteresis loop and results in a marked increase in the band gap energy from 3.21 to 3.31 eV. This could be of potential significance for the activity of the catalyst. The modification of hysteresis classification by the incorporation of a nonpolar cosolvent in the synthesis process relays valuable information about the viability of morphological reconstruction of pores. Table 1 provides a summary of mesoporous TiO_2-SiO_2 materials prepared with varying solvent to cosolvent volume ratios and calcined at 500 °C.

The reasons for significant improvements in the surface areas with the inclusion of a cosolvent are still under significant debate and scrutiny. However, Ranjit and Klabunde[34] postulate that the presence of a cosolvent in a mesoporous system affects the hydrolysis and condensation processes, and the hydrophobicity of the solvent reduces the surface tension of the pore walls, leading to less collapse of the pores and ultimately to a more open and porous material. We believe that a similar situation arises in the TiO_2-SiO_2 materials where the involvement of substituted aromatic solvents initiates weak intermolecular interactions that facilitate the branching and expansion of the structural framework and produces highly porous materials as a result. Table 1 indicates that the average pore diameter of the TiO_2-SiO_2 materials prepared using nonpolar solvents increases. Importantly, the results also indicate that the nature and the amount of the nonpolar solvent have an influence on the textural properties of the resulting calcined TiO_2-SiO_2 materials.

3.3. Effect of the Calcination Temperature on the TiO_2-SiO_2 Mesostructure. TiO_2-SiO_2 prepared solely in ethanol, catalyzed by concentrated HNO_3, and calcined at 500 °C demonstrated amorphicity, as indicated previously in Figure 1. These materials were also calcined at 600 and 800 °C, and our powder X-ray diffractometry results (not shown) indicate enhanced crystallinity upon calcination at higher temperatures. The TiO_2-SiO_2 materials calcined at 500 °C show very broad peaks, whereas the samples calcined at 600 and 800 °C show sharp and narrow peaks indicative of higher crystallinities. In order to see if the crystallinity trends are applicable in other pH ranges, we used aqueous NH_3 as the catalyst for the preparation of TiO_2-SiO_2. Three catalysts were prepared similar to the method described previously, but aqueous NH_3 was used instead of concentrated HNO_3. These materials were calcined at 500, 600, and 800 °C, and the results are shown in Figure 6A. Calcination at 500 °C exhibits broad diffraction peaks of due to d_{101}, d_{004}, d_{200}, d_{105}, and d_{204} at 25.2, 37.9, 48.1, 55.1, and 62.8°, indicating that the TiO_2-SiO_2 materials possess only the anatase phase of TiO_2. The peaks gradually become more pronounced and intense as the calcination temperature is increased to 600 and 800 °C while still maintaining the anatase phase. This feature is confirmed by an increase in intensity of the Raman spectra, as discussed previously in Figure 4, alluding to improved crystallinity. In summary, TiO_2-SiO_2 materials prepared either in acid or basic medium in the presence of only ethanol as the solvent and calcined at 500 °C are fairly amorphous, whereas materials calcined at 600 and 800 °C are relatively highly crystalline. This trend is also observed for other TiO_2-SiO_2 materials prepared in an acid medium but employing cosolvents such as toluene, *p*-xylene, and so forth.

A slight red-shift in the absorption band reflects a change in the effective band gap energy from 3.36 to 3.23 eV (Figure 6B) when the calcination temperature is increased from 500 to 800 °C, thus deducing that the change in crystallite size was minimal.

3.4. Effect of the TiO_2/SiO_2 Ratio in the Mesostructure. The effect of TiO_2/SiO_2 ratio was investigated by preparing two sets of samples. The first set consisting of four samples (TS04, TS10, TS11, and TS12) was prepared by using ethanol/toluene (1:1 v/v ratio) but by varying the TiO_2/SiO_2 ratios. As indicated in Table 1, the surface area progressively increase from 423.3 m^2/g for a TiO_2/SiO_2 ratio of 1:1 to 671.1 (TiO_2/SiO_2 ratio = 1:2), 671.5 (TiO_2/SiO_2 ratio = 1:3), and 1033 m^2/g (TiO_2/SiO_2 ratio = 1:4). A concurrent increase in the pore volume is also observed as the amount of silica increases. Catalysts were also prepared using the ethanol-only system (TS01, TS13, TS14, and TS15), and a similar trend in the textural properties was observed, as illustrated in Table 1. In summary, our results indicate that high surface areas and large pore volumes can be realized by increasing

dx.doi.org/10.1021/jp110988j |*J. Phys. Chem. C* 2011, 115, 6126–6135

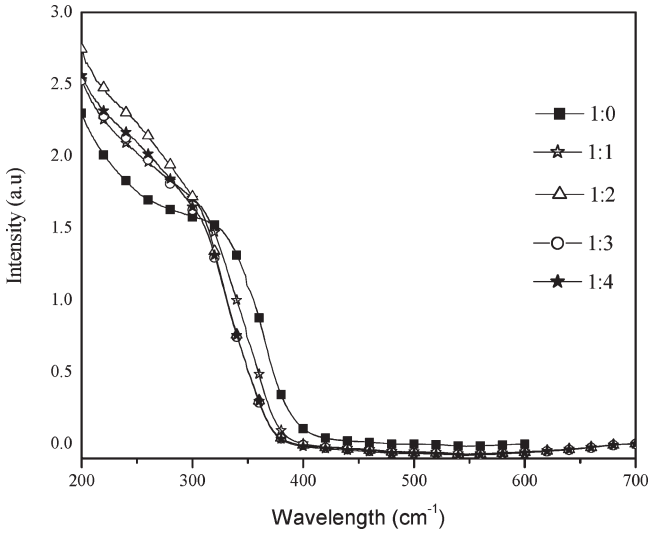

Figure 7. DR spectra of TiO_2-SiO_2 mixed oxide materials synthesized with an ethanol to toluene ratio of 1:1 while varying the TiO_2/SiO_2 ratio.

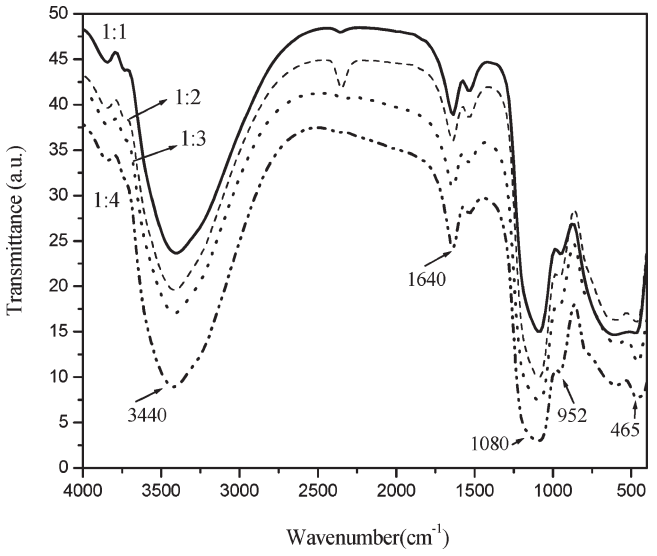

Figure 8. FT-IR spectra of calcined TiO_2-SiO_2 mixed oxide materials derived from gelation with an ethanol to toluene ratio of 1:1 while varying the titania to silica ratio.

the silica amount (correlating with a decrease in titania amount) in the mixed oxides.

Figure 7 shows the UV−vis DR spectra of TiO_2-SiO_2 materials prepared with different TiO_2/SiO_2 ratios in the presence of ethanol/toluene (1:1 v/v ratio). The DR spectra indicate that a decrease in titania loading causes a slight shift in the absorption band toward shorter wavelengths. This shift can be attributed to the size quantization effect arising from small particle sizes and/or dispersion of the TiO_2 species.[35] A similar trend was also observed for TiO_2-SiO_2 materials prepared with different TiO_2/SiO_2 ratios in the presence of ethanol only as the solvent.

The IR spectra in Figure 8 provide additional information about the lattice vibrations of the TiO_2-SiO_2 mixed oxides. The weak band at 952 cm^{-1} can be associated with the Ti−O−Si heterolinkages, which indirectly suggests the interaction between TiO_2 and SiO_2 at the molecular scale.[15,36] This peak becomes less pronounced from ratios 1:1 to 1:4 probably due to the decrease in TiO_2 content.

The most intense band in the spectrum at 1080 cm^{-1} is assigned to asymmetric mode of the Si−O−Si stretching vibration with bridging oxygen.[37] The 465 cm^{-1} band is more prevalent in the TiO_2/SiO_2 ratio of 1:3 and corresponds to the Si−O−Si bending mode. Weak absorption characteristics of the scissor bending mode of physisorbed water are evidenced by a band at 1640 cm^{-1}, while vibration at 3440 cm^{-1} is ascribed to a deformation mode of physisorbed molecular water due to the adsorptive nature of TiO_2-SiO_2 materials.[18,38] The broad adsorption band between about 2700 and 3700 cm^{-1} corresponds to the fundamental stretching vibrations of different surface hydroxyl groups emerging from Ti−OH and $Ti-OH_2$ species vibrating at 3200 and 3400 cm^{-1}, respectively.[39] The broad absorption at 3440 cm^{-1} is also composed of a superposition of Si−O−H stretching vibrations and O−H stretching of a hydrogen-bonded molecular water.

3.5. Intermolecular Chemistry of the Mixed Oxide Matrix. The surface and physisorption properties are essential for the overall activity of these hydrothermally synthesized mixed oxide materials in heterogeneous photocatalytic systems. SiO_2 is an ideal support because its transparency to UV irradiation ensures the uninterrupted exposure of titanium sites to the light.[40] The activity however depends on the titanium content introduced to the Si alkoxide precursor like tetraethylorthosilicate $Si(OC_2H_5)_4$, that is, TEOS, to improve the surface acidity and provide extra binding sites for the interaction of organic substrates.[41] Due to extremely slow hydrolysis of TEOS[42] and the rapid hydrolysis of the Ti alkoxides, that is, $Ti(OCH(CH_3)_2)_4$, prehydrolysis of the Si alkoxide was necessary to enable homogeneous mixing of the precursors. It has been determined that the introduction of organic solvents influences the hydrolysis and condensation reaction kinetics by altering intermolecular interactions that in turn affect the overall gelation and precipitation processes. Prehydrolysis in an alcohol medium promotes solvation through alkoxy bridging[43] and enhances coordination expansion by use of polar solvents or alcohol in the polymerization process. However, these media may result in rapid precipitation and the formation of a highly condensed product.[44] Modification by use of nonpolar solvents has emerged as an alternative to alkoxy bridging in order to achieve coordination expansion,[45,46] with postulations that the initial hydrolysis of the Ti alkoxide precursor is affected by the presence of toluene due to insolubility forcing the rapid attack of water on titanium.[24,34] This consequently changes the kinetics of gelation, hastening the hydrolysis and producing more porous gels of high surface area in a limited time, as observed in this study. On the contrary, Bains argues that the conjugated π-system could enable the aromatic cosolvent to act as a weak donor solvent toward the titanium alkoxide and slow down the hydrolysis process by dissociating the complexes, hence improving the molecular mixing.[47] Turova and co-workers seem to be in agreement by hypothesizing a mechanism through which oligomerization is enhanced in aromatic solvents probably due to partial breakage of alkoxide bridges and the subsequent formation of n-complexes thus leading to polymeric gels.[48] Brinker contributes to the argument by reaffirming the possibility of alkoxy bridging playing a role in the stable oligomerization in the nonpolar solvent medium, vital for the control of the hydrolysis and condensation kinetics of transition-metal alkoxides.[43] A similar phenomenon can be concluded in our study from the

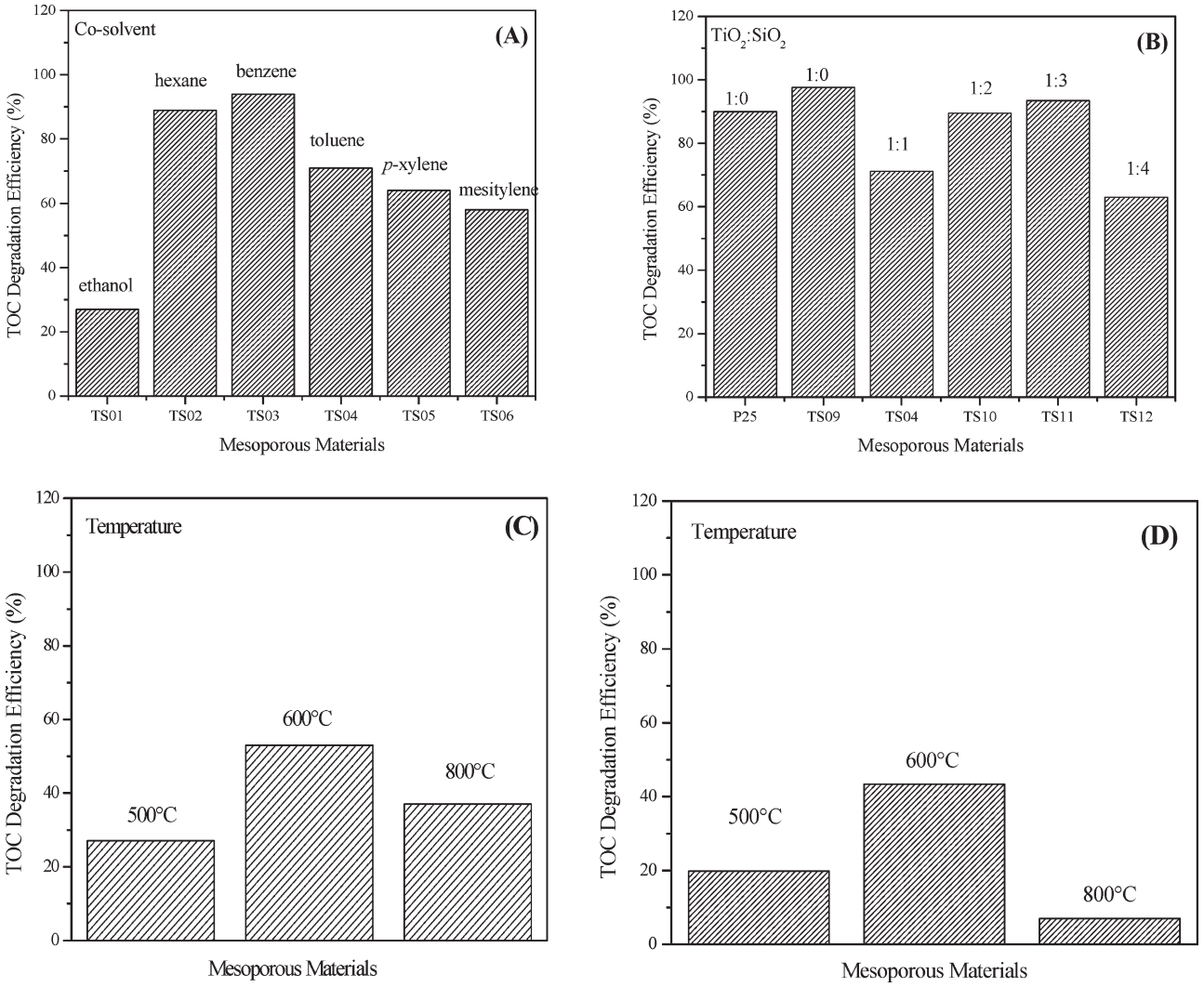

Figure 9. Evaluation of the photocatalytic activity of TiO_2-SiO_2 mixed oxides by TOC determination. All synthesized materials have ethanol/cosolvent = 1:1. The TiO_2/SiO_2 is maintained at 1:1, and the effect of the nature of cosolvent is analyzed with TS01, TS02, TS03, TS04, TS05, and TS06 containing ethanol, hexane, benzene, toluene, *p*-xylene, and mesitylene as cosolvents, respectively (A). The TiO_2/SiO_2 ratio is then varied, resulting to TS09 (TiO_2/SiO_2 = 1:0), TS10 (TiO_2/SiO_2 = 1:2), TS11 (TiO_2/SiO_2 = 1:3), and TS12 (TiO_2/SiO_2 = 1:4) (B). Calcination temperatures of 500, 600, and 800 °C were imparted on an ethanol−toluene system catalyzed by aq. NH_3 (C), and the photocatalytic efficiencies are compared to that of an ethanol-only system catalyzed by concd HNO_3 (D).

formation of highly porous gels that exhibit a Ti−O−Si linkage IR feature, characteristic of homogeneous mixing.

3.6. Activity of TiO_2-SiO_2 Mixed Oxides for Phenol Degradation. TiO_2-SiO_2 mixed oxides possess activity with total organic carbon (TOC) degradation efficiencies superior to commercial Evonik Degussa P 25 and comparable to bare TiO_2. This may be attributed to interplay of several properties such as surface area and porosity, crystallinity, and dispersion of TiO_2 crystallites. A combination of these parameters is believed to readily avail more active sites to toxic organic pollutants for degradation.

Anderson and Bard have attributed enhanced performance to larger surface areas due to enhanced adsorption of organic substrates to the surface of the catalyst. Our investigations clearly indicate that the introduction of aromatic cosolvent such as toluene results in larger surface areas, enhanced from 282.1 (ethanol only) to ∼425 m^2/g (ethanol/cosolvent = 1:1) and average pore geometries from 30.66 to 68.89 Å, as illustrated in Table 1. Improved catalytic efficiencies for all cosolvent-induced samples are also evident in Figure 9A. The cosolvent results in a broad pore size distribution, facilitating the diffusion of the organic substrate into a variety of more accessible pores. Benzene and toluene produce materials of similar surface area of ∼423 m^2/g but possess significantly different activity. Furthermore, the use of benzene as the cosolvent results in a material with higher degradation efficiency than the other cosolvent-induced materials. We believe that the high activity is due to the relatively higher crystallinity of this material because the textural properties such as surface area, pore volume, and average pore diameter of this material are comparable with that of materials prepared with cosolvents such as toluene, *p*-xylene, mesitylene, and so forth.

Powder XRD results (not shown) indicate that the TiO_2-SiO_2 mixed oxide prepared using benzene and calcined at 500 °C is considerably more crystalline than corresponding materials prepared using other cosolvents and calcined at the same temperature. This indicates the role of crystallinity to be an

dx.doi.org/10.1021/jp110988j |*J. Phys. Chem. C* 2011, 115, 6126–6135

important factor in determining the photocatalytic efficiencies in the TiO_2-SiO_2 mixed oxides. Our hypothesis is validated by photocatalytic studies of TiO_2-SiO_2 mixed oxides prepared using different ethanol to toluene ratios (1:1, 2:1, and 1:2). The photocatalytic activities of these materials (TS04, TS07, and TS08) were found to be similar although their surface areas and porosities varied. The powder XRD results of these three materials indicate their crystallinities to be very similar, suggesting that it influenced the photocatalytic activity significantly compared to other parameters such as surface area, pore volume, or average pore diameter.

The prominence of crystallinity was further investigated by studying the effect of varying the TiO_2/SiO_2 ratio on the photocatalytic activities of cosolvent-induced TiO_2-SiO_2 mixed oxides. The degradation efficiencies of these materials are slightly lower than bare TiO_2 (TS09), as depicted in Figure 9B. The surface area of the TiO_2 (65 m^2/g) is very low compared to that of TiO_2-SiO_2 mixed oxides (423−1033 m^2/g); however, its photocatalytic activity is higher, as noted previously, and is comparable with a commercial Evonik Degussa P 25 sample. The powder XRD results of TS09 (not shown) indicate the crystallinity to be significantly higher (ca. three times) compared with that of the mixed oxide samples, once again highlighting the importance of crystallinity in influencing the photocatalytic activity. It is imperative to observe that increasing the silica amounts results in a progressive improvement in catalytic activity, peaking at an optimum TiO_2/SiO_2 ratio of 1:3 with degradation efficiencies comparable to that of bare TiO_2. Catalytic activity is however offset with more amounts of SiO_2 probably due to anatase crystals that are well-dispersed and occluded in the SiO_2 amorphous phases. Therefore, the presence of TiO_2 at an optimum ratio of 1:3 is notable in determining the effective dispersion of TiO_2 within the silica framework. The small anatase crystals dispersed on the surface of the SiO_2 provide a large surface area to volume ratio, which improves the exposure of electrons and holes for the reaction with organic substrates. It has been determined that a small crystallite size is beneficial for enhanced photoactivity, and hindering the growth can be achieved by the surrounding SiO_2 phase that ensures stabilization of the anatase.[22,49] The diffusion between anatase crystallites is minimized, which in effect suppresses the rate of nucleation (growth) of the crystallite size.[5] In addition, the increase in photoactivity has been attributed to the presence of a mixed Ti−O−Si coordination at the interface region that serves to activate the oxidation of organic substrates via strong Brønsted acid sites.[49] This coordination involves the integration of tetrahedral Ti species into a tetrahedral SiO_2 matrix and creating charged oxygen atoms.

$$Ti{-}O^- + Si - OH \rightarrow Ti - O - Si + OH^-$$

A charge imbalance created is then bridged by hydroxyl groups, resulting in the Brønsted acidity. In essence, an optimal amount of SiO_2 ensures a favorable dispersion of anatase crystals in the mesostructure that allows for the emergence of more Ti−O−Si coordination sites responsible for higher degradation efficiencies.

The materials prepared in this study were subject to different conditions to further investigate the scope of crystallinity. During the optimization of the gel synthesis media, a material catalyzed by aqueous basic NH_3 (ethanol/toluene = 1:1) and another prepared in the ethanol-only system (TS01) resulted in XRD patterns typical of highly amorphous materials. The results depicted in Figure 9C and D indicate low activity in TiO_2-SiO_2 mixed oxides calcined at 500 °C, which may be due to the low crystalline nature of the mesostructure. The activity is enhanced when crystallinity is optimized by an increment in calcination temperature to 600 °C. However, there is a decline in activity at 800 °C, suggesting a slight destruction of the mesostructure by the high temperature or the agglomeration of the anatase crystallites.

These observations suggest an inquiry into the origin of crystalline features as we attempt to support crystallinity as a significant feature for enhanced activity in TiO_2-SiO_2 mixed oxides. Recent research has shown that amorphous TiO_2 possesses very low photoactivity, which improves markedly upon mild thermal treatment due to the formation of crystalline phases. Preliminary experiments in our laboratory also indicate low photocatalytic efficiency for TiO_2-SiO_2 mixed oxide materials synthesized at ambient temperature conditions. Without hydrothermal treatment, procedures identical to the preparation of TS04 (ethanol/toluene), TS05 (ethanol/*p*-xylene), and TS06 (ethanol/mesitylene) were followed. TOC degradation efficiencies of resulting photocatalysts were 4, 12, and 8% compared to those of HTS that yielded 71, 64, and 58%, respectively. Although this crystallization process enhancement during mild hydrothermal treatment of mixed oxide materials is indeterminate, we can infer from Bein and co-workers, who utilized electron microscopy in conjunction with in situ DLS and XRD to image the development of crystalline structure within amorphous gel particles. Wang also concurs that porous structures with minimal defects can be sythnesized by HTS under appropriate conditions to ensure complete sol−gel reaction.[9] During this low-temperature treatment at 120 °C, random nuclei grow into a regular crystal lattice owing to reversible condensation reactions that beak M−O−M bonds and harness the attraction of energetically favorable coordination of oxy-species.[25] This treatment provides a mechanism through which TiO_2 and SiO_2 species interact and eventually have increased framework TiO_2 content. The synthesis procedure in this study therefore entails a cosolvent that provides large porosities, in which optimal amounts of SiO_2 can effectively disperse the highly crystalline anatase achieving more Ti−O−Si coordination sites for the efficient photocatalytic degradation of phenol to its relatively less toxic byproducts. Kinetics and mechanistic studies by liquid chromatography are underway to understand the interactions between the catalyst and the pollutant. Preliminary studies identify benzoquinone, hydroxybenzoquinone, and hydroxyhydroquinone as the main degradation products and are consistent with the TOC results.

4. CONCLUSION

Highly active TiO_2-SiO_2 mixed oxide materials have been successfully prepared in mild acidic conditions by HTS via CIG by using select nonpolar aromatic cosolvents. The TiO_2 to SiO_2 ratio was optimized to 1:3 to produce the most active photocatalyst because higher titania loadings lead to agglomeration that enhances the growth in the size of particles, resulting in lower catalytic activity. Owing to the high surface areas of all catalysts prepared under similar conditions while varying titania content, it can be concluded that the improved photoactivity is dependent on three concurrent factors, that is, the availability of active sites by optimizing the anatase content, the utilization of suitable cosolvents to enhance dispersion of anatase in the silica

framework, and the ability of the combination of the HTS and optimum calcination temperature to maximize the crystallinity of the anatase species. It is imperative to acknowledge the influence of simple nonpolar aromatic cosolvents like toluene in accelerating the gelation thus yielding highly active porous mesoporous materials synthesized for the photocatalytic degradation of phenol.

AUTHOR INFORMATION

Corresponding Author

*E-mail: Harrison.Kibombo@usd.edu (H.S.K.); Tel: 605-677-6189. Fax: 605-677-6397. E-mail: Ranjit.Koodali@usd.edu.

ACKNOWLEDGMENT

We extend sincere gratitude to NSF-CHE-0619190, NSF-CHE-0722632, NSF-EPS-0903804, DE-EE0000270, DE-FG02-08ER64624, and the State of SD for funding this project. We also acknowledge Dr. Sarah Chadima and Dr. Chaoyang Jiang of the University of South Dakota for their assistance with XRD and Raman studies, respectively.

REFERENCES

(1) Mills, A.; Lee, S. *J. Photochem. Photobiol. A: Chem.* **2002**, *152*, 233–247.
(2) Young, J. A. *J. Chem. Educ.* **2007**, *84*, 759.
(3) Fox, M. A.; Dulay, M. T. *Chem. Rev.* **1993**, *83*, 341–357.
(4) Herrmann, J. M. *Top. Catal.* **2005**, *34*, 49–65.
(5) Anderson, C.; Bard, A. J. *J. Phys. Chem. B* **1997**, *101*, 2611–2616.
(6) Gao, X.; Wachs, I. E. *Catal. Today* **1999**, *51*, 233–254.
(7) Kang, C.; Jing, L.; Guo, T.; Cui, H.; Zhou, J.; Fu, H. *J. Phys. Chem. C* **2008**, *113*, 1006–1013.
(8) Dagan, G.; Sampath, S.; Lev, O. *Chem. Mater.* **1995**, *7*, 446–453.
(9) Wang, C.; Ying., J. Y. *Chem. Mater.* **1999**, *11*, 3113–3120.
(10) Miller, J. B.; Ko, E. I. *Catal. Today* **1997**, *35*, 269–292.
(11) Pabon, E.; Retuert, J.; Quijada, R.; Zarate, A. *Microporous Mesoporous Mater.* **2004**, *67*, 195–203.
(12) Rupp, W.; Husing, N.; Schubert, U. *J. Mater. Chem.* **2002**, *12*, 2594–2596.
(13) Coles, M. P.; Lugmair, C. G.; Terry, K. W.; Tilley, D. T. *Chem. Mater.* **2000**, *12*, 122–131.
(14) Davis, R. J.; Liu, Z. *Chem. Mater.* **1997**, *9*, 2311–2324.
(15) Li, Y.; Kim, S. *J. Phys. Chem. B* **2005**, *109*, 12309–12315.
(16) Theurich, J.; Lindner, M.; Bahnemann, D. W. *Langmuir* **1996**, *12*, 6368–6376.
(17) Dutoit, D. C. M.; Schneider, M.; Baiker, A. *J. Catal.* **1995**, *153*, 165–176.
(18) Mikushina, Y. V.; Shishmakov, A. B.; Matskevich, V. V.; N. A. Russ, Z. *J. Inorg. Chem.* **2008**, *53*, 1557–1560.
(19) Jeong, J.; Park, J.; Choi, S.; Lee, K.; Lee, C. *Bull. Korean Chem. Soc.* **2007**, *28*, 2288–2292.
(20) Fu, X.; Clark, L. A.; Yang, Q.; Anderson, M. A. *Environ. Sci. Technol.* **1996**, *30*, 647–653.
(21) Kumar, S. R.; Suresh, C.; Vasudevan, A. K.; Suja, N. R.; Mukundan, P.; Warrier, K. G. K. *Mater. Lett.* **1999**, *38*, 161–166.
(22) Xu, Y.; Zheng, W.; Liu, W. *J. Photochem. Photobiol. A: Chem.* **1999**, *122*, 57–60.
(23) Murata, C.; Yoshida, H.; Kumagai, J.; Hattori, T. *J. Phys. Chem. B* **2003**, *107*, 4364–4373.
(24) Ranjit, K. T.; Martyanov, I.; Demydov, D.; Uma, S.; Rodrigues, S.; Klabunde, K. J. *J. Sol−Gel Sci. Technol.* **2006**, *40*, 335–339.
(25) Mintova, S.; Olson, N. H.; Bein, T. *Angew. Chem., Int. Ed.* **1999**, *38*, 3201–3204.
(26) Testino, A.; Bellobono, I. R.; Buscaglia, V.; Canevali, C.; D'Arienzo, M.; Polizzi, S.; Scotti, R.; Morazzoni, F. *J. Am. Chem. Soc.* **2007**, *129*, 3564–3575.
(27) Kominami, H.; Yukishita, K.; Kimura, T.; Matsubara, M.; Hashimoto, K.; Kera, Y.; Ohtani, B. *Top. Catal.* **2008**, *47*, 155–161.
(28) Kim, E. Y.; Whang, C. M.; Lee, W. I.; Kim, Y. H. *J. Electroceram.* **2006**, *17*, 899–902.
(29) Tian, G.; Fu, H.; Jing, L.; Xin, B.; Pan, K. *J. Phys. Chem. C* **2008**, *112*, 3083–3089.
(30) Wu, Z. Y.; Tao, Y. F.; Lin, Z.; Liu, L.; Fan, X. X.; Wang, Y. *J. Phys. Chem. C* **2009**, *113*, 20335–20348.
(31) Kruk, M.; Jaroniec, M. *Chem. Mater.* **2001**, *13*, 3169–3183.
(32) Lowell, S.; Shields, J. E.; Thomas, M. A.; Thommes, M. *Characterization of Porous Solids and Powders: Surface Area, Pore Size and Density*; Academic Press Inc: San Diego, CA, 1990; p 13.
(33) Mariscal, R.; Lopez-Granados, M.; Fierro, J. L. G.; Sotelo, J. L.; Martos, C.; Van Grieken, R. *Langmuir* **2000**, *16*, 9460–9467.
(34) Ranjit, K. T.; Klabunde, K. *J. Chem. Mater.* **2005**, *17*, 65–73.
(35) Yamashita, H.; Kawasaki, S.; Ichihashi, Y.; Harada, M.; Takeuchi, M.; Anpo, M. *J. Phys. Chem. B* **1998**, *102*, 5870–5875.
(36) Ren, J.; Li, Z.; Liu, S.; Xing, Y.; Xie, K. *Catal. Lett.* **2008**, *124*, 185–194.
(37) Dirken, P. J.; Smith, M. E.; J.; Whitfield, H. J. *J. Phys. Chem.* **1995**, *99*, 395–401.
(38) Xu, J.; Liping, L.; Yan, Y.; Wang, H.; Wang, X.; Fu, X.; Li, G. *J. Colloid Interface Sci.* **2008**, *318*, 29–34.
(39) Ryczkowski, J. *Catal. Today* **2001**, *68*, 263–381.
(40) Alemany, L. J.; Banares, M. A.; Pardoa, E.; Martina, F.; Galán-Fereres, M.; Blasco, J. M. *Appl. Catal. B* **1997**, *13*, 289–297.
(41) Choi, W. *Catal. Surv. Asia* **2006**, *10*, 16–28.
(42) Chang, C.; Fogler, H. S. *Langmuir* **1997**, *13*, 3295–3307.
(43) Brinker, J. C.; Scherer, G. W. *Sol−Gel Science: The Physics and Chemistry of Sol−Gel Processing*; Academic Press Inc: San Diego, CA, 1990; p 524.
(44) Livage, J.; Henry, M.; Sanchez, C. *Prog. Solid State Chem.* **1998**, *18*, 292.
(45) Nabavi, M.; Doeuff, S.; Sanchez, C.; Livage, J. *J. Non-Cryst. Solids* **1990**, *121*, 31–34.
(46) Turova, N. Y.; Turevskaya, E. P.; Kessler, V. G.; Yanovskaya, M. I. *The Chemistry of Metal Alkoxides*; Kluwer Academic Publisher: Norwell, MA, 2002; p 85.
(47) Bains, M. S.; Bradley, D. C. *Can. J. Chem.* **1962**, *40*, 2218–2228.
(48) Turova, N. Y.; Turevskaya, E. P.; Yanovskaya, M. I.; Yanovsky, A. I.; Kessler, V. G.; Tcheboukov, D. E. *Polyhedron* **1998**, *17*, 899–915.
(49) Hirano, M.; Ota, K.; Inagaki, M.; Iwata, H. *J. Ceram. Soc. Jpn.* **2004**, *112*, 143–148.